Scientific Research Journal,
Vol 17, No 2 (2020) 191-207
https://doi.org/10.24191/srj.v17i2.10136

Silicon Substituted Lithium Stannum Phosphate Ceramic Electrolytes: Structural, Electrical and Electrochemical Properties

Noriah Ab Wahab[1], Nurul Akmaliah Dzulkurnain[2], Nur Amalina Mustaffa[1]*, Nor Sabirin Mohamed[3]

[1]Faculty of Applied Sciences, Universiti Teknologi MARA, 40450 Selangor, Malaysia.
[2]School of Chemical Sciences, Faculty of Science and Technology, Universiti Kebangsaan Malaysia, Malaysia.
[3]Centre for Foundation Studies in Science, University of Malaya, 50603 Kuala Lumpur, Malaysia.

**Corresponding author's e-mail: nuramalina@uitm.edu.my*

Received: 20 July 2020
Accepted: 26 August 2020
Online First: 28 August 2020

ABSTRACT

Structural, electrical, and electrochemical properties of silicon (Si) substituted NASICON-structured lithium stannum phosphate, $Li_{1+y}Sn_2P_{3-y}Si_yO_{12}$ with $0 < y < 1$ that was prepared by the low-temperature water-based sol-gel method has been investigated. From the structural analysis, all samples in the system from y = 0.1 to 0.5 displayed rhombohedral $R\bar{3}c$ symmetry. The electrical analysis showed that the total ionic conductivity, was increased with the increase of silicon content, y. A high ionic conductivity value of 6.05×10^{-5} S cm^{-1} exhibited at y = 0.5 with a temperature of 500 °C. Linear sweep voltammetry analysis of the highest conducting sample showed that the sample was electrochemically stable up to 5.1 V. Meanwhile, the ionic transference number value of the sample was 0.99, suggesting that the majority of mobile charge carriers were predominantly due to ions. Thus, from these results, it indicated that silicon substitution in $LiSn_2P_3O_{12}$ ceramic electrolytes is significantly enhanced the electrical and electrochemical properties.

Keywords: *NASICON; solid electrolytes; sol-gel; impedance analysis*

INTRODUCTION

Over the past few years, the revolution of technologies was rising with a variety of combustion reactions. As a result, the usage of energy has gradually increased the demands in the utilisation of fossil fuels, which had to threaten our mother nature [1]. Therefore, lithium-ion batteries have been invested as a solution to overcome environmental pollution and energy shortage issues [2]. For the last few years, it begins to show its benefits through various breakthroughs [3]. Later, to increase the productivity of battery, many types of rechargeable batteries have been developed. Among them, the rechargeable lithium-ion battery has been pointed as one of the accessible energy storage device technology for varied applications such as mobile phones, laptops, tablets, and electric vehicles because of its high energy density and exceptional cycling life [4-5]. However, the lithium-ion battery has safety issues such as overcharging, overheating, or short circuits that may result in fire or explosion due to the flammable liquid electrolyte in the commercial battery. So, an ideal and suitable solid electrolyte with low electronic conductivity, high conductivity at a higher temperature, and wider electrochemical stability windows are required as an alternative. [6].

All solid-state-lithium ion batteries have been widely studied due to the inherent advantages of inorganic solid electrolytes in terms of safety and reliability [7]. Among solid electrolytes, NASICON (Sodium Superionic Conductor) type ion conductors have been tested widely in energy applications, for instance, in batteries, electric vehicles, sensors, etc. [8]. According to Hong (1976), high ion conductivity and stability of phosphate units are advantages of NASICON over other electrolyte materials [9]. Among the batteries, those based on lithium shows the best performance.

Lithium analogous sodium (Na) superionic conductor (NASICON) [6-7] with the general formula of $LiM_2P_3O_{12}$ with M = Ge, Ti, Hf, Zr, Sn, etc. are solid electrolytes with increasing interest to be utilised in high energy solid-state battery. The basic structure of the NASICON material is rhombohedral $R\bar{3}c$ that consists of a three-dimensional framework of corner-shared ZrO_6 octahedra and PO_4 tetrahedra. $LiSn_2P_3O_{12}$ also possesses NASICON structure [8–12], but the ionic conductivity reported was still low, $\sim 10^{-7}$ S cm^{-1} and $\sim 10^{-10}$ S cm^{-1} [8–12]. However, we managed to obtain the ionic conductivity value in the order of 10^{-5} S cm^{-1} at 500 °C using a water-

based sol-gel method [13-14]. Therefore, to enhance the ionic conductivity of the $LiSn_2P_3O_{12}$ compound, partial substitution can be carried out in both Sn and P sites. In this case, it can be carried out by partially substituting at P^{5+} (0.38 Å) site $^{4+}$ site using tetravalent ion, Si^{4+} (0.72 Å), in the goal of creating Li^+ interstitial ions where $P^{5+} \rightarrow Li^+ + Si^{4+}$. As such, a water-based sol-gel method was used to synthesize a new $Li_{1+y}Sn_2P_{3-y}Si_yO_{12}$ compound. Then the effects of Si^{4+} substitution on $LiSn_2P_3O_{12}$, the structural, electrical and electrochemical properties of the ceramic electrolytes were studied using X-ray diffraction (XRD), impedance spectroscopy (IS), ionic transference number measurements and linear sweep voltammetry (LSV).

EXPERIMENTAL PROCEDURES

$Li_{1+y}Sn_2P_3$-$ySiyO_{12}$ with $0 < y < 1$ samples were synthesized via water-based sol-gel method where y ranging from 0.1 to 0.5. Sample for $y = 0.1$ is labeled as SI1, y = 0.3 is labeled as SI3 and $y = 0.5$ is labeled as SI5. All the chemicals are analytical grade and directly used as received without further purification. For $LiSn_2P_3O_{12}$ sample preparation, lithium acetate (CH_3COOLi), stannum (IV) chloride pentahydrate ($SnCl_4.5H_2O$), and ammonium phosphate ($H_{12}N_3O_4P$) were used as starting materials with citric acid ($C_6H_80_7$) as the chelating agent while distilled water as the solvent. For silicon substituted samples, silicon dioxide (SiO_2) was added to the starting materials. Firstly all the starting materials were dissolved in distilled water under magnetic stirring. The citric acid ($C_6H_8O_7$), polyethylene glycol ($C_2H_6O_2$) and ammonium hydroxide (NH_4OH) were then mixed to the previously prepared solution under magnetic stirring. The molar ratio of $C_2H_6O_6$: NH_4OH was 1:1. After the solution was transferred into a reflux system, it was continuously stirred for 24 hours until the homogenous solution formed. Then, the solution was taken out ad vaporised for about four hours under magnetic stirring at 80°C to obtain the gel. The obtaining gels were dried in an oven for 24 hours at 150°C.

Before the precursor powder was sent for the sintering process, it was ground for 30 minutes to obtain a fine powder. Then, all the samples were sintered at 600 °C for 48 hours, and the final product was then ground again for 30 minutes. Specac hydraulic press under a pressure of 5 tons was used to press the powder to form a 13mm of diameter with a thickness of 1.00 - 3.00

mm of pallets. Structural analysis of the samples was then evaluated by XRD using a PaNalytical – X'pert^3 x-ray diffractometer with Cu-K_α radiation of a wavelength of 1.5406 Å and 0.026 ° in step size. Impedance measurements of all the sintered pellets were determined by AC impedance spectroscopy using Solatron 1260 Impedance analyzer over a frequency range from 1 to 10 MHz at the temperature range from 30 to 500°C. The electrochemical stability windows of the electrolytes system were performed by LSV using the Wonatech ZIVE MP2 multichannel electrochemical workstation at a scan rate of 5 mV s^{-1} at room temperature. The ionic transference number measurement was evaluated by Wagner's D.C polarisation technique using the Wonatech ZIVE MP2 multichannel electrochemical workstation by applying a potential of 0.5 V, and the current was monitored as a function of time until it reached a steady-state condition at room temperature.

RESULTS AND DISCUSSIONS

Figure 1 shows the X-ray diffraction patterns of $Li_{1+y}Sn_2P_{3-y}Si_yO_{12}$ samples. The spectra indicate the presence of rhombohedral $R\bar{3}c$ $LiSn_2P_3O_{12}$ crystalline phase in all the samples which are well-matched with the peak positions assigned in standard JCPDS file. SnO_2 impurity is also observed in all samples showing the presence of unreacted cassiterite SnO_2 [18]. However, the maximum value of substitution, *y*, is only up to 0.5. When *y* exceeded 0.5, certain peaks disappeared, and the samples become less crystalline with the existence of SnO_2 impurity peaks. As such, further analysis was conducted only on SI1, SI3, and SI5 samples.

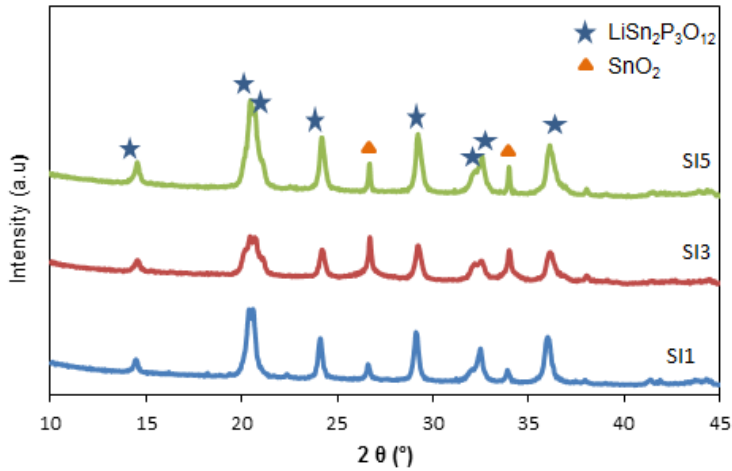

Figure 1: X-ray Diffraction Patterns of $Li_{1+y}Sn_2P_{3-y}Si_yO_{12}$ System

Furthermore, the peaks in the range 23° to 25° were analysed to determine the existence of the Si^{4+} content in the $LiSn_2P_3O_{12}$ crystal lattice, as shown in Figure 2. The diffraction peaks shifts to higher diffraction angle when Si^{4+} ion is in the $LiSn_2P_3O_{12}$ structure. This indicates that Si^{4+} was successfully substituted into the crystal lattice of $LiSn_2P_3O_{12}$ rather than forming other phases or impurities. Furthermore, no peak associated with silicon was detected in the XRD spectra, indicating Si^{4+} was successfully inserted into the $LiSn_2P_3O_{12}$ structure instead of creating impurities. All peaks are sharp and well defined, suggesting that the compounds are generally well crystallised.

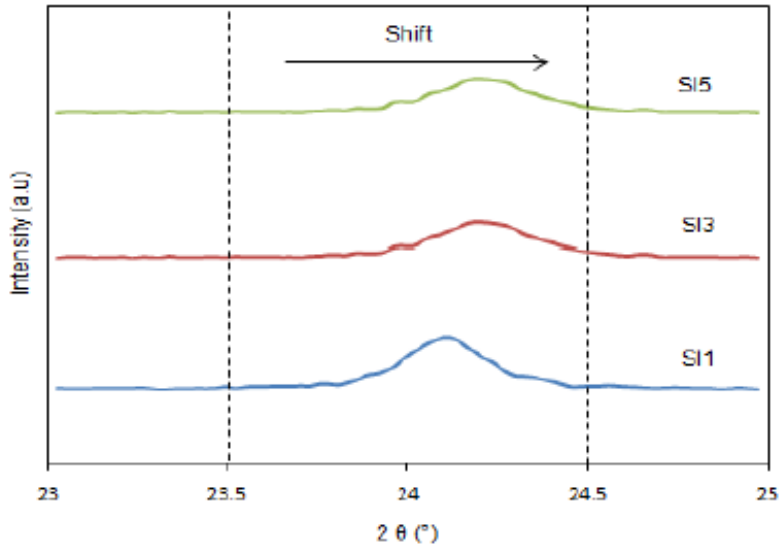

Figure 2: X-ray Diffractograms of $Li_{1+y}Sn_2P_{3-y}Si_yO_{12}$ System in 2θ Range from 23.0 to 25.0°

Meanwhile, the list of lattice parameters and crystallite size for the $Li_{1+y}Sn_2P_{3-y}Si_yO_{12}$ samples are listed in Table 1. The values of *a, c* and *V* increase as the value of y increases. Moreover, the crystallite size also shows the same trend and increases due to the substitution of larger ionic radius of Si^{4+} ion (r_{ion} = 0.40Å) compared to P^{5+} ion (r_{ion} = 0.38 Å). Besides, the addition of Si^{4+} ions simultaneously increase the production of Li^+ ions. Thus, the adjustment in the lattice parameter will provide short diffusion Li^+ distances which cause an improvement in increasing rate capability of compound [19]

Table 1: Lattice Parameters and Unit Cell Volume of $Li_{1+y}Sn_2P_{3-y}Si_yO_{12}$ System

Sample	a [Å]	c [Å]	V [Å 3]	Crystallite size [Å]
SI1	8.4277	21.6033	1329.71	124.72
SI3	8.4351	21.6136	1332.68	128.89
SI5	8.4406	21.6753	1338.23	132.51

Impedance spectroscopy is a useful method to resolve the contributions of various processes such as bulk, grain boundary, and electrode effect in the specified frequency domain. As such, for impedance measurement, all three samples were chosen based on the XRD analysis. The selected sample of $Li_{1+y}Sn_2P_{3-y}Si_yO_{12}$ (SI1, SI3, and SI5) was sintered at 30 °C and 500°C, as it was more convenient to compare those results. Figure 3 shows that, at 30 °C or room temperature, the plots consist of two overlapping semicircles with a spike at the low-frequency area for all samples, SI1, SI3, and SI5. The semicircles that occurred at the high-frequency region is corresponding to bulk response with its intercept at the *x*-axis allocated to bulk resistance, R_b Furthermore, the spike in the low frequency is due to the processes occurring at the electrode and electrolyte interface [16-17]. Besides, as *y* increases from 0.1 to 0.5, R_b and R_{gb} values decrease, suggesting an enhancement in ionic conductivity.

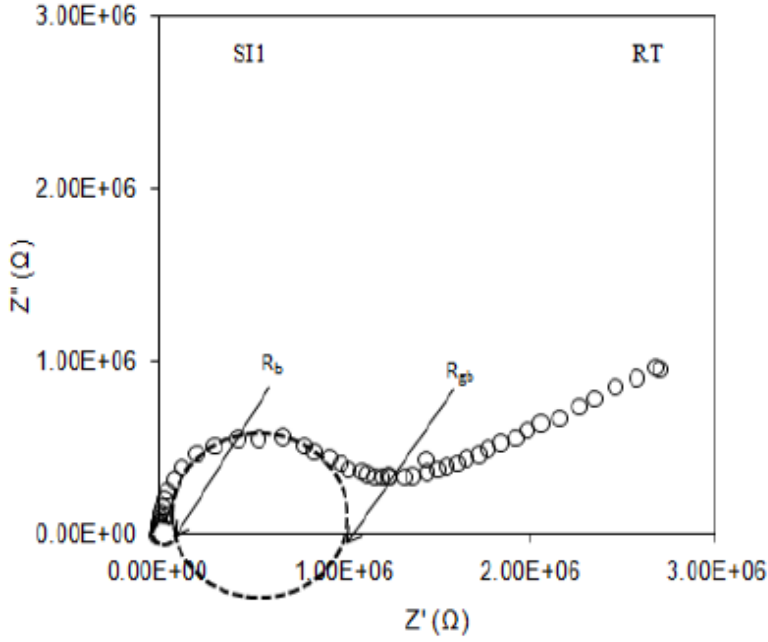
SI1
RT
3.00E+06
2.00E+06
1.00E+06
0.00E+00
Z'' (Ω)
R_b
R_{gb}
0.00E+00
1.00E+06
2.00E+06
3.00E+06
Z' (Ω)

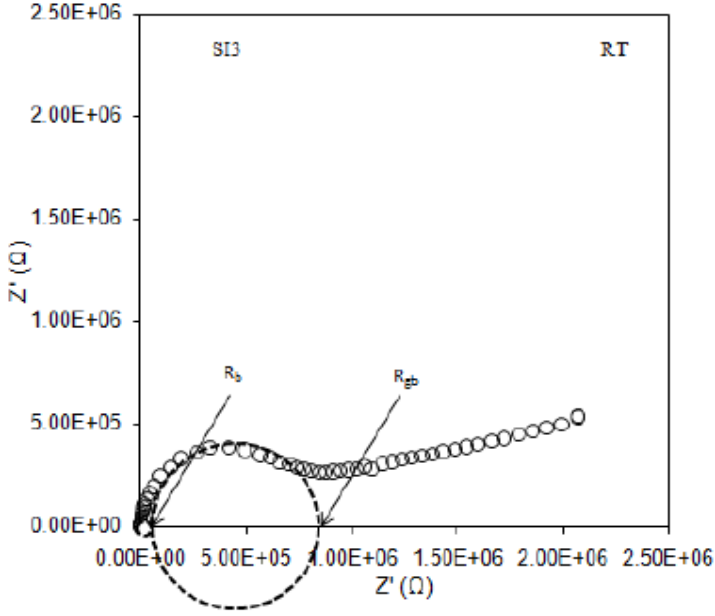
SI3
RT
2.50E+06
2.00E+06
1.50E+06
1.00E+06
5.00E+05
0.00E+00
Z' (Ω)
R_b
R_{gb}
0.00E+00
5.00E+05
1.00E+06
1.50E+06
2.00E+06
2.50E+06
Z' (Ω)

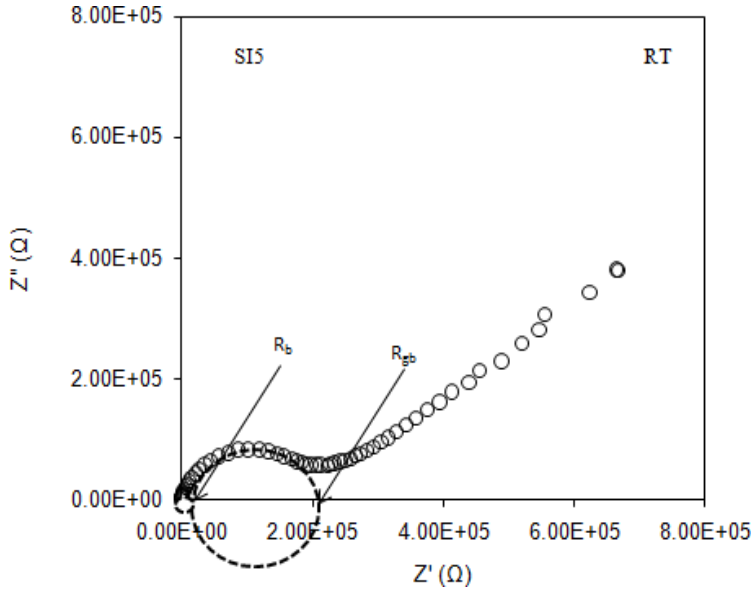

Figure 3: Complex Impedance Plot of SI1, SI3, and S15 at Room Temperature

Meanwhile, as the temperature increases from 30 °C to 500 °C, only one semicircle, which is R_b, and spike at lower frequency area were detected, as shown in Figure 4 for the SI5 sample. The plot shows a similar trend for sample SI1 and SI3 at 500°C. In this plot, the spike can be associated with the characteristics of electrode polarisation effects due to the accumulation of ions between the electrode and samples [22].

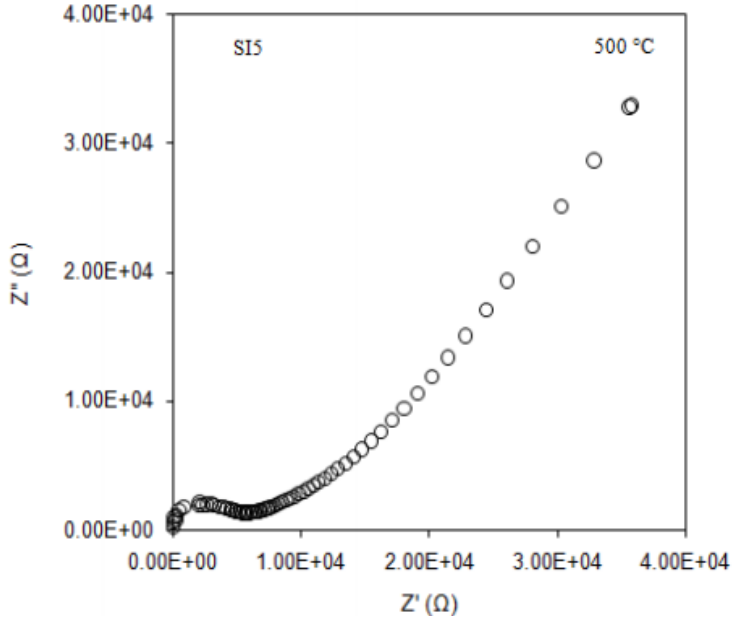

Figure 4: Complex Impedance Plot of SI5 at 500 °C

The value of σ_b, σ_{gb}, and σ_t for all samples are listed in Table 2. When Si^{4+} was substituted into the parent compound, total conductivity, σ_t at room temperature was increased by one order of magnitude as a result of the increment of the grain boundary conductivity, σ_{gb}. However, at 500 °C, the conductivity is still at the same order of magnitude. The highest conductivity found is 6.05×10^{-5} S cm^{-1} at 500 °C for the SI5 sample. Therefore, the rise of the ionic conductivity in Si^{4+} substituted samples mainly originates from grain boundary conductivity, not from bulk conductivity. Besides that, additional Li^+ is introduced by substituting P^{5+} by Si^{4+} and is located in an energetically favored site (M3). This occupation induces the nearest-neighboring M1 site to displace towards the next M3 site, which promotes an interstitial migration mechanism [23].

On top of that, the increase in σ_b can be most probably attributed to increasing amounts of Li^+ occupying the M3 sites and displacing the Li^+ in M1 sites towards the nearest-neighboring M3 sites. Therefore, the additional Li content further promotes the Li^+ diffusion and increases the conductivity

in the system [24]. The change in the lattice parameter and volume of the samples can also improve the conductivity since it changes the bottleneck size, which results in the mobility of ion[25].

The enhancement in ionic conductivity obtained in this study was resulted from the framework distortion due to the replacement of the larger Si ion (r_{ion} = 0.40 Å) for, the smaller P ion (r_{ion} = 0.38 Å). This distortion alters the local electron density of adjacent phosphorous atoms due to a lower electronegativity of Si (1.90) compared with P (2.19). It affects the lithium-ion dynamics and consequently affects its bulk conductivity.

Table 2: Ionic Conductivities Value for $Li_{1+y}Sn_2P_{3-y}Si_yO_{12}$ System

Sample	$\sigma_{b'500}$ (S cm^{-1})	$\sigma_{b'30}$ (S cm^{-1})	$\sigma_{gb'30}$ (S cm^{-1})	$\sigma_{t,500}$ (S cm^{-1})	$\sigma_{t,30}$ (S cm^{-1})
SI1	9.43 ×10^{-6}	2.17 ×10^{-6}	2.22 ×10^{-7}	9.43 ×10^{-6}	2.01 ×10^{-7}
SI3	1.51 ×10^{-5}	2.58 ×10^{-6}	3.02 ×10^{-7}	1.51 ×10^{-5}	2.70 ×10^{-7}
SI5	6.05 ×10^{-5}	8.09 ×10^{-6}	1.20 ×10^{-6}	6.05 ×10^{-5}	1.05 ×10^{-6}

Linear sweep voltammogram was used to study the decomposition voltage of the sample. Linear sweep voltammetry analysis for the highest conducting sample, sample SI5 in Figure 5 showed that the decomposition voltage of the sample is at 5.1 V at room temperature. This means that Si^{4+} substituted samples also possessed a 6.3% wider voltage stability window compared to the unsubstituted sample. It also exhibits an electrochemical stability window more than 4.5 V [26] and suggests that the sample is stable enough to be applied as solid electrolytes in electrochemical devices.

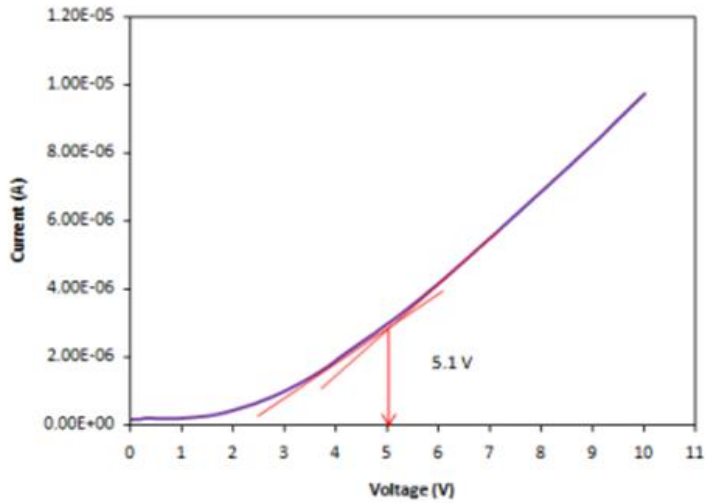

Figure 5: Linear Sweep Voltammogram of Sample SI5

Meanwhile, in Figure 6, the ionic transference number value of the sample was 0.99, suggesting that the majority of mobile charge carriers were ions [27]. The total ionic transference number value is close to unity, which is 0.99, confirming that the conductivity is a result of ionic mobility rather than electronic mobility [27]. The ingfinding suggests that compounds with high transference numbers can withstand the negative effects of concentration polarisation [28]. From these two results, it shows that this sample is suitable to be used as solid electrolytes in the electrochemical device application with the appropriate choice of the electrode.

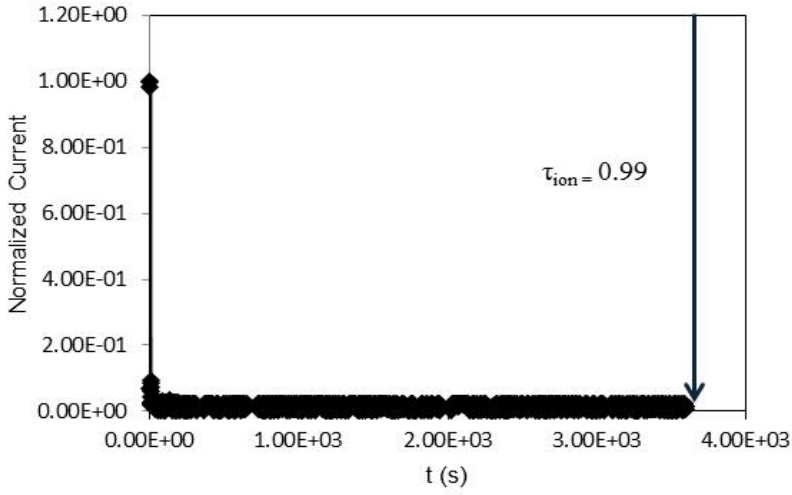

Figure 6: Typical Plot of Normalised Polarisation Current versus Time for Sample SI5

CONCLUSIONS

The effects of Si^{4+} substitution on $LiSn_2P_3O_{12}$ to the structure, conductivity, and electrochemical stability window were successfully reported. XRD analysis confirmed the formation of rhombohedral $R\bar{3}c$ phase of $LiSn_2P_3O_{12}$ samples with no peak associated with silicon indicating that Si^{4+} were successfully inserted into the $LiSn_2P_3O_{12}$ structure. Si^{4+} substituted sample showed the highest ionic conductivity value at 500 °C that was 6.05×10^{-5} S cm^{-1} for the sample with $y = 0.5$. The highest conductivity value can be associated with the excess of interstitial Li^+ ions, the increment of the crystallinity of the sample, and the change of bottleneck size suitable for the mobility of ion. Besides that, the Si^{4+} substitution sample also possessed high ionic transference number value and promising decomposition voltage, which indicates that it is suitable for electrochemical device application.

ACKNOWLEDGEMENTS

The authors would like to extend their gratitude towards Universiti Teknologi MARA and the University of Malaya for allowing this research to be carried out. This research was supported by the Lestari Grant (600-IRMI/MyRA 5/3/LESTARI (050/2017)) provided by Universiti Teknologi MARA (UiTM).

REFERENCES

[1] M. Armand & J. M. Tarascon, 2008. Building better batteries. *Nature, 451*(7179), pp. 652-657. DOI: 10.1038/451652a

[2] M. Hou, F. Liang, K. Chen, Y. Dai, & D. Xue, 2020. Challenges and perspectives of NASICON-type solid electrolytes for all-solid-state lithium batteries. *Nanotechnology, 31*(13), p. 132003. DOI: 10.1088/1361-6528/ab5be7.

[3] M. Armand, & J. M. Tarascon, 2001. Nature Lithium Battery. *Nature, 414*(11), pp. 359–367. DOI: 10.1038/35104644.

[4] M. Kotobuki, & M. Koishi, 2015. Sol–gel synthesis of $Li_{1.5}Al_{0.5}Ge_{1.5}(PO_4)_3$ solid electrolyte. *Ceramics International, 41*(7), pp. 8562-8567.

[5] T. Pareek, S. Dwivedi, S. A. Ahmad, M. Badole, & S. Kumar, 2020. Effect of NASICON-type $LiSnZr(PO_4)_3$ ceramic filler on the ionic conductivity and electrochemical behavior of PVDF based composite electrolyte. *Journal of Alloys and Compounds, 824*, p. 153991. https://doi.org/10.1016/j.jallcom.2020.153991

[6] N. A. Dzulkurnain, N. A. Mustaffa & N. S. Mohamed, 2017. Structural, Electrical and Electrochemical Properties of $Mg_{0.55}Si_{1.9}Al_{0.1}Fe_{0.1}(PO_4)_3$ Ceramic Electrolytes. *Journal of New Materials for Electrochemical Systems, 20*(3) pp. 89-149. https://doi.org/10.14447/jnmes.v20i3.269

[7] Z. Luo, C. Qin, Y. Wu, W. Xu, S. Zhang, & A. Lu, 2020. Structure and properties of Fe_2O_3-doped $50Li_2O10B_2O_3$-$40P_2O_5$ glass and glass-ceramic electrolytes. *Solid State Ionics, 345*, p. 115177.

[8] L. Vijayan, & G. Govindaraj, 2012. NASICON Materials: Structure and Electrical Properties. *Polycryst. Mater. - Theor. Pract. Asp.* DOI: 10.5772/28967.

[9] J. B. Goodenough, H. P. Hong, & J. A. Kafalas, 1976. Fast Na^+-ion transport in skeleton structures. *Materials Research Bulletin, 11*(2), pp. 203-220. https://doi.org/10.1016/0025-5408(76)90077-5

[10] H. P. Hong, 1976. Crystal structures and crystal chemistry in the system Na_{1+x} Zr_2 Six P_{3-x}-O12. *Materials Research Bulletin, 11*(2), pp. 173-182. https://doi.org/10.1016/0025-5408(76)90073-8

[11] A. Martinez, J. M. Rojo, J. E. Iglesias, J. Sanz, & R. M. Rojas, 1994. Formation process of $LiSn_2(PO_4)_3$, a monoclinically distorted NASICON-type structure. *Chemistry of materials, 6*(10), pp. 1790-1795. https://doi.org/10.1021/cm00046a036

[12] A. Martinez-Juarez, R. Jimenez, P. Duran-Martin, J. Ibañez, & J. M. Rojo, 1997. Effect of the phase transition of on the ion conduction in-Teflon composites. *Journal of Physics: Condensed Matter, 9*(20), p. 4119.

[13] J. E. Iglesias, J. Sanz, A. Martínez-Juárez, & J. M. Rojo, 1997. Low-temperature triclinic distortion in NASICON-type$LiSn_2(PO_4)_3$.

[14] A Martinez-Juarez, J. M. Rojo, J. E. Iglesias, & J. Sanz, 1995. Reversible monoclinic-rhombohedral transformation in $LiSn_2(PO_4)_3$ with NASICON-type structure. *Chemistry of Materials, 7*(10), pp. 1857-1862. https://doi.org/10.1021/cm00058a016

[15] M. G. Lazarraga, J. Ibañez, M. Tabellout, & J. M. Rojo, 2004. On the aggregation process of ceramic $LiSn_2P_3O_{12}$ particles embedded in Teflon matrix. *Composites Science and Technology, 64*(5), pp. 759-765.

[16] N. A. Mustaffa, & N. S. Mohamed, 2015. Properties of stannum-based Li-NASICON-structured solid electrolytes for potential application in electrochemical devices. *Int J Electrochem Sci, 10*, pp. 5382-5394.

[17] N. A. Mustaffa, S. B. R. S. Adnan, M. Sulaiman, & N. S. Mohamed, 2015. Low-temperature sintering effects on NASICON-structured $LiSn_2P_3O_{12}$ solid electrolytes prepared via citric acid-assisted sol-gel method. *Ionics, 21*(4), pp. 955-965. DOI:10.1007/s11581-014-1257-2

[18] W. J. Cui, J. Yi, L. Chen, C. X. Wang, & Y. Y. Xia, 2012. Synthesis and electrochemical characteristics of NASICON-structured $LiSn_2(PO_4)_3$ anode material for lithium-ion batteries. *Journal of Power Sources, 217*, pp. 77-84. https://doi.org/10.1016/j.jpowsour.2012.05.117

[19] M. Ershadi, M. Javanbakht, S. A. Mozaffari, D. Brandell, M. T. Lee, & B. Zahiri, 2020. Facile stitching of graphene oxide nanosheets with ethylenediamine as three dimensional anode material for lithium-ion battery. *Journal of Alloys and Compounds, 818*, p. 152912. https://doi.org/10.1016/j.jallcom.2019.152912

[20] J. T. Irvine, D. C. Sinclair, & A. R. West, 1990. Electroceramics: characterization by impedance spectroscopy. *Advanced Materials, 2*(3), pp. 132-138. https://doi.org/10.1002/adma.19900020304

[21] S. Kumar, & P. Balaya, 2016. Improved ionic conductivity in NASICON-type $Sr^{(2+)}$ doped $LiZr_2(PO_4)_3$. *Solid State Ionics, 296*, pp. 1-6. https://doi.org/10.1016/j.ssi.2016.08.012

[22] C. R. Mariappan, & G. Govindaraj, 2005. Conductivity and ion dynamic studies in the $Na_{4.7x}\ Ti_{(1.3-x)}(PO_4)_{(3.3-x)}$ ($0 \leq x \leq 0.6$) NASICON material. *Solid State Ionics, 176*(13-14), pp. 1311-1318.

[23] B. Lang, B. Ziebarth, & C. Elsässer, 2015. Lithium ion conduction in $LiTi_2P_3O_{12}$ and related compounds based on the NASICON structure: a first-principles study. *Chemistry of Materials, 27*(14), pp. 5040-5048.

[24] D. Rettenwander, A. Welzl, S. Pristat, F. Tietz, S. Taibl, G. J. Redhammer, & J. Fleig, 2016. A microcontact impedance study on

NASICON-type $Li_{(1+x)}$ Al_x $Ti_{(2-x)}$ $(PO_4)_3$ ($0 \leq x \leq 0.5$) single crystals. *Journal of Materials Chemistry A, 4*(4), pp. 1506-1513.

[25] C. M. Chang, Y. I. Lee, S. H. Hong, & H. M. Park, 2005. Spark Plasma Sintering of $LiTi_2$ P_3O_{12} - Based Solid Electrolytes. *Journal of the American Ceramic Society, 88*(7), pp. 1803-1807. https://doi.org/10.1111/j.1551-2916.2005.00246.x

[26] A. D. Robertson, A. R. West, & A. G. Ritchie, 1997. Review of crystalline lithium-ion conductors suitable for high temperature battery applications. *Solid State Ionics, 104*(1-2), pp. 1-11. https://doi.org/10.1016/S0167-2738(97)00429-3

[27] A. G. Jolley, G. Cohn, G. T. Hitz, & E. D. Wachsman, 2015. Improving the ionic conductivity of NaSiCon through aliovalent cation substitution of $Na_3Zr_2Si_2PO_{12}$. *Ionics, 21*(11), pp. 3031-3038. https://doi.org/10.1007/s11581-015-1498-8

[28] K. A. Dwelle, & A. P. Willard, 2020. The limited influence of transference number on the performance of nanoscale batteries. *The Journal of Chemical Physics, 152*(7), 074702